2011

Dynamic nucleosome-depleted regions at androgen receptor enhancers in the absence of ligand in prostate cancer cells

Claudia Andreu-Vieyra
University of Southern California

John Lai
University of Southern California

Benjamin P. Berman
University of Southern California

Baruch Frenkel
University of Southern California

Li Jia
Washington University School of Medicine in St. Louis

See next page for additional authors

Recommended Citation

Andreu-Vieyra, Claudia; Lai, John; Berman, Benjamin P.; Frenkel, Baruch; Jia, Li; Jones, Peter A.; and Coetzee, Gerhard A., ,"Dynamic nucleosome-depleted regions at androgen receptor enhancers in the absence of ligand in prostate cancer cells." Molecular and Cellular Biology.31,23. 4648-4662. (2011).
http://digitalcommons.wustl.edu/open_access_pubs/2266

Authors

Claudia Andreu-Vieyra, John Lai, Benjamin P. Berman, Baruch Frenkel, Li Jia, Peter A. Jones, and Gerhard A. Coetzee

Dynamic Nucleosome-Depleted Regions at Androgen Receptor Enhancers in the Absence of Ligand in Prostate Cancer Cells

Claudia Andreu-Vieyra, John Lai, Benjamin P. Berman, Baruch Frenkel, Li Jia, Peter A. Jones and Gerhard A. Coetzee

	Updated information and services can be found at: http://mcb.asm.org/content/31/23/4648
	These include:
REFERENCES	This article cites 48 articles, 13 of which can be accessed free at: http://mcb.asm.org/content/31/23/4648#ref-list-1
CONTENT ALERTS	Receive: RSS Feeds, eTOCs, free email alerts (when new articles cite this article), more»

Journals.ASM.org

Dynamic Nucleosome-Depleted Regions at Androgen Receptor Enhancers in the Absence of Ligand in Prostate Cancer Cells[▽]

Claudia Andreu-Vieyra,[1]† John Lai,[1]† Benjamin P. Berman,[2] Baruch Frenkel,[3] Li Jia,[4]
Peter A. Jones,[1] and Gerhard A. Coetzee[1]*

*Department of Urology,[1] Epigenome Center,[2] and Departments of Orthopedic Surgery and of Biochemistry and Molecular Biology,[3]
Keck School of Medicine, University of Southern California, Los Angeles, California 90089, and Center for Pharmacogenomics,
Department of Internal Medicine, Washington University School of Medicine, St. Louis, Missouri 63110[4]*

Nucleosome positioning at transcription start sites is known to regulate gene expression by altering DNA accessibility to transcription factors; however, its role at enhancers is poorly understood. We investigated nucleosome positioning at the androgen receptor (AR) enhancers of *TMPRSS2*, *KLK2*, and *KLK3/PSA* in prostate cancer cells. Surprisingly, a population of enhancer modules in androgen-deprived cultures showed nucleosome-depleted regions (NDRs) in all three loci. Under androgen-deprived conditions, NDRs at the *TMPRSS2* enhancer were maintained by the pioneer AR transcriptional collaborator GATA-2. Androgen treatment resulted in AR occupancy, an increased number of enhancer modules with NDRs without changes in footprint width, increased levels of histone H3 acetylation (AcH3), and dimethylation (H3K4me2) at nucleosomes flanking the NDRs. Our data suggest that, in the absence of ligand, AR enhancers exist in an equilibrium in which a percentage of modules are occupied by nucleosomes while others display NDRs. We propose that androgen treatment leads to the disruption of the equilibrium toward a nucleosome-depleted state, rather than to enhancer *de novo* "remodeling." This allows the recruitment of histone modifiers, chromatin remodelers, and ultimately gene activation. The "receptive" state described here could help explain AR signaling activation under very low ligand concentrations.

Nucleosomes are the basic units of eukaryotic chromatin, each one containing ∼146 bp of DNA wrapped around an octamer of histone core proteins, which in turn are separated by linker DNA sequences of variable length (39). Nucleosomes play a pivotal role in chromatin structure, and their differential occupancy at promoters (transcription start sites) regulates gene expression by altering DNA accessibility (39). For instance, a nucleosome-depleted region (NDR) at transcriptional start sites correlates with gene expression, whereas the positioning of a nucleosome over the transcriptional start site results in gene repression (23). In contrast, the role of nucleosome positioning at other regulatory regions, particularly distal ones such as enhancers, is less well characterized. Interestingly, nucleosome turnover was recently shown to be increased at genes and regulatory elements (9), suggesting that this process may control nucleosome density and the existence of NDRs.

Enhancers are nondirectional regulatory elements that control promoter activity at a distance on linear DNA. Several histone marks, including mono- and dimethylated H3K4 (H3K4me1 and H3K4me2) and acetylated H3K9,14 (AcH3), have been shown to correlate or be associated with regions that display enhancer activity, although H3K4me2 and AcH3, along with the trimethylation version of H3K4 (H3K4me3), are also located at transcriptional start sites (16, 44). Enhancers generally contain DNA recognition motifs for transcription factors which, upon binding, regulate gene expression by looping to the transcriptional start sites of their target genes.

The androgen receptor (AR) is a ligand-dependent nuclear receptor that plays a major role in prostate cancer onset and progression (10). The AR is recruited primarily to enhancers together with transcriptional collaborators, which include the transcription factors GATA-2, FOXA1, and OCT1/2 (43). Once an enhancer-protein complex is formed, it communicates with gene promoter regions through looping, thereby affecting transcription over large linear DNA distances (41). Using ChIP-Seq, we have recently demonstrated that androgen-treated prostate cancer (LNCaP) cells show the expected strong AR occupancy at the enhancers of kallikrein 3/prostate-specific antigen (KLK3/PSA) and KLK2 (3). Interestingly, two well-positioned nucleosomes containing AcH3 were shown to flank AR-occupied regions in androgen-treated cells (3). A similar bimodal pattern of histone modifications relative to transcription factor binding sites at enhancers has been observed in KCl-stimulated murine neurons for H3K4me1 and CREB binding protein (25) and in LNCaP cells for H3K4me2 and AR (14). Using H3K4me2 ChIP-Seq data from LNCaP cells and prediction algorithms, He et al. (14) suggested that AR binding sites at enhancers are occupied by a well-positioned nucleosome, which is then destabilized and presumably removed or shifted by the addition of androgens and AR occupancy. However, this suggestion was based on data generated by micrococcal nuclease (MNase) I digestion and chromatin immunoprecipitation (ChIP) analysis of modified histone tails; the extent of nucleosome occupancy was unclear.
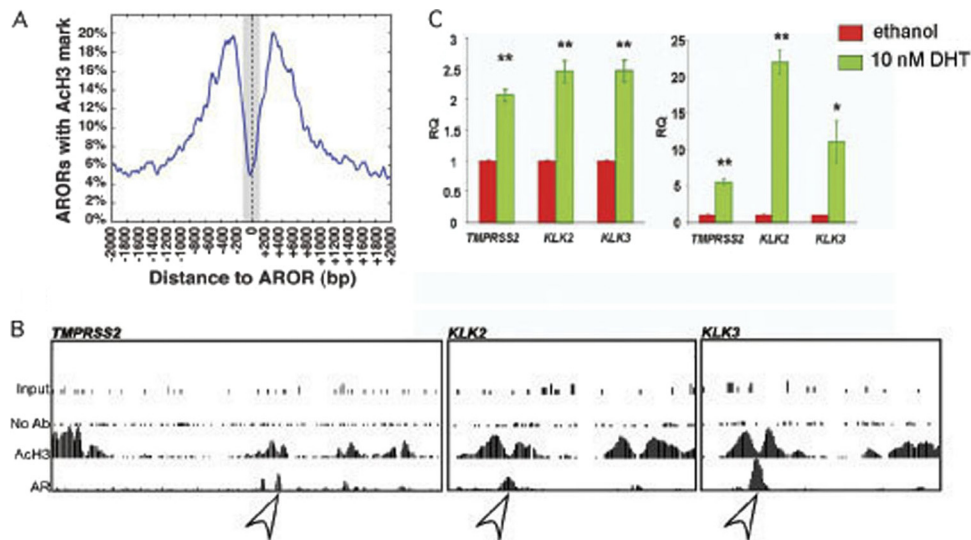

FIG. 1. Acetylated H3 flanks AR-occupied regulatory regions in LNCaP cells. (A) Genome-wide ChIP-Seq analysis shows 20% histone H3 enrichment surrounding AR-occupied regions (ARORs) in DHT-treated LNCaP cells. (B) ChIP-Seq profiles for recruitment of the AR and histone H3 acetylated at Lys-9 and Lys-14 (AcH3) at the enhancers of three prototypical androgen-responsive genes (*TMPRSS2*, *KLK2*, and *KLK3*). No-Ab and input controls are also shown. (C) qPCR analysis of *TMPRSS2*, *KLK2*, and *KLK3* mRNA levels after 4 h (left panel) or 16 h (right panel) of treatment with 10 nM DHT. Bars show expression relative to GAPDH levels (RQ) and represent the average of 3 independent experiments ± the SEM. *, $P < 0.05$; **, $P < 0.01$.

To characterize the chromatin architecture in AR-occupied regions, we used a combination of ChIP-Seq, ChIP-qPCR (quantitative PCR), and a highly sensitive single-molecule nucleosome occupancy and methylome sequencing (NOMe-Seq) assay. Here we show that in androgen-depleted LNCaP and LAPC4 cells, a percentage of the enhancer modules of the three well-known AR targets KLK3/PSA, KLK2, and transmembrane protease serine 2 (TMPRSS2) displayed an NDR at the AR binding site. In addition, the AR collaborator GATA-2 was present at the NDR in androgen-deprived cells. Interestingly, knockdown of *GATA-2* resulted in loss of the NDR at the *TMPRSS2* enhancer but not at the *KLK3* and *KLK2* enhancers in the absence of hormone. These results suggest that GATA-2 plays a role in maintaining NDRs in a locus-specific manner. Treatment with androgen resulted in AR occupancy and in increases in the number of enhancer modules displaying NDRs at all three enhancers. The NDRs overlapped precisely with the AR binding regions. We propose a model whereby, in the absence of ligand, a single nucleosome at AR enhancers turns over more rapidly than surrounding ones, resulting in a number of enhancer modules without the nucleosome at any given time, while others are occupied by a nucleosome. Under these conditions, pioneer factors such as GATA-2 play a role in maintaining this turnover equilibrium. We further propose that upon androgen treatment and the resulting AR occupancy, the turnover rates of nucleosomes are altered to favor the nucleosome-depleted state, resulting in an increased number of modules displaying NDRs at any given time. This, in turn, may facilitate the recruitment of histone modifiers to give rise to histone acetylation and methylation at flanking nucleosomes, ultimately leading to AR target gene expression.

MATERIALS AND METHODS

Cell culture. The prostate cancer cell line LNCaP and the IMR90 (human fibroblasts) cell line were obtained from the American Type Culture Collection (Manassas, VA). The prostate cancer cell line LAPC4 was a kind gift from Charles Sawyers (UCLA, Los Angeles, CA). IMR90 cells (passages 4 to 7) were maintained in Dulbecco's modified Eagle's medium supplemented with 10% fetal bovine serum (FBS). LNCaP cells (passages 25 to 46) were maintained in phenol red-free RPMI 1640 containing 5% charcoal/dextran-stripped FBS (Gemini, Woodland, CA) for 3 or 7 days prior to a 0.5-h, 2-h, 4-h, or 16-h treatment with 10 nM 5-α-dihydrotestosterone (DHT; Sigma Chemical Co., St. Louis, MO) or ethanol-treated control. LAPC4 cells were grown in phenol red-free RPMI 1640 containing 5% charcoal/dextran-stripped FBS for 2 days prior to a 4-h 10 nM DHT or ethanol treatment.

ChIP-Seq. LNCaP cells were treated for 4 h with 10 nM DHT after hormone deprivation for 3 days. ChIP was carried out as previously described (20), using antibodies against AcH3 and AR. Chromatin was fragmented to a size range of 200 to 400 bases with a Fisher Sonic Dismembrator. ChIP DNA was prepared into libraries and sequenced using the Illumina Genome Analyzer II according to the manufacturer's protocols. We collected 15,963,583 (AR), 18,957,344 (AcH3), and 17,079,409 (no antibody [Ab]) uniquely alignable 36-bp single end reads from the Illumina Genome Analyzer IIx. Alignments were performed using MAQ, and we used only reads with a unique mapping quality score of 30 or greater. ChIP-Seq data tracks were generated by averaging read densities at 50-bp intervals (average reads per kbp). Because single-end sequencing was used, we extended each tag by 250 bp in the appropriate direction. Peaks were identified by examining average read counts in all such 500-bp windows and selecting all with 15 or more reads within the window (30 reads per kbp). Based on randomly distributed reads under the binomial distribution, windows with 15 or more reads are extremely unlikely to occur by chance (P values of 4.4^{E-11}, 3.8^{E-10}, and 8.3^{E-11} for AR, AcH3, and no Ab, respectively). Significant windows were merged if they were within 100 bp of each other, yielding 4,762 highly significant peaks for AR and 579 for the no-Ab control. A total of 405 AR peaks overlapped no-Ab peaks and were removed, to yield 4,357 final AR peaks. The fraction of AR peaks overlapped by an AcH3 peak (Fig. 1) was quantified by aligning AcH3 peaks with the center of each AR peak.

ChIP analysis and ChIP-qPCR. LNCaP cells were maintained in phenol red-free RPMI 1640 containing 5% charcoal/dextran-stripped FBS for 3 days prior to 4 h of treatment with 10 nM DHT or an ethanol-treated control. ChIP was carried out as described previously (20), using 4 μg of antibodies

TABLE 1. ChIP and NOMe-Seq primer sets used in this study

Primer application and name	Sequence (5′ to 3′)	
	Forward	Reverse
ChIP		
KLK3/PSA[a]		
R1	GCCCACCTGTTTGTCAGTAACTC	ATGAACCTCATGCTGTCTGCTAAG
R2	CAGACAGCATGAGGTTCATGTTCA	TGTGCACAGCATCCACCTAGAC
R3	ATACTGGGACAACTTGCAAACCT	CAGGCTTGCTTACTGTCCTAGATAA
R4	GGTGTTGCTGTCTTTGCTCAGAA	GGTGGAAGGCTCTGGCTGAA
R5	TGCAGGACAGTCTCAACGTTCC	ACCCAGAAGTTCTGATCCCCA
KLK2		
R1	AGAAATTATGGCTGGATGTCTCTG	GAGATTATGATGGGCTCCTGGT
R2	CCACAGCTAAGGAGGCAGCA	CCATCCACCTGAACTGCTCTGA
R3	GGTTGAAAGCAGACCTACTCTGG	AGATCTAGGTTTGCTTACTGCCTTAG
R4	CCATCTTGCAAGGCTATCTGCTG	TGTGTCTTCTGAGCAAAGGCAAT
R5	CTAACCAAGATTTCTAGGTCCAGTTC	CACTCAAGCCCAGAAGTTCTGAT
TMPRSS2		
R1	CCCTGTTTGTGGGGCTGTTC	CTGCCTCCCTCTGGGTTCTG
R2	CACTGCTGTCAACTCCACGG	CTGTGTTCGGACCTGTTAGAGTTAT
R3	GTGGCCCACCACTTCCTCAC	CACACAGCAAGGCAGAGGACA
R4	TTAGACAACAAATGGCCACCTG	GTTGGAGCTAGTGCTGCATGTC
R5	CTCTAACTACAGCCCAGGCAAGT	AGCAAGGGCAGTTTAGCCAG
R6	CTCTAACTACAGCCCAGGCAAGT	AGCAAGGGCAGTTTAGCCAG
NOMe-Seq		
KLK3/PSA[a]		
R1	ATTTTTATTATGATATTAGGATTTTATTGTATTT	CACCTTTTTTTTTCTAAATTATTATTTC
R2	AGAGTTTATGAGATTTTTGAGTT	CTCACTCAAACCCAAAAATTCTAATC
KLK2		
R1	TTTAGATTTTGATTTTGAGGTTATTTTAGATTTTT	CAATATTAAAAAACAATTTTCCATAATTCTCTTATA TTTC
R2	TGGTAGAATTTATGAGATTTTTGGGTT	CAAAAATTCTAATCCCCACCCATATC
TMPRSS2		
R1	TTATTTTGGTTTTTTTTAGTTTTATTAAATTTTAGT	CTTATAACACTTCACCCATCTTTAACATATAC
R2	TTTTTTTTATTATTTAGGATTAATATTTTTAT	CCTATCTTTTATAATTCCCCTTTATAATCTATATTGT
TMPRSS2 (single amplicon), R1	TTTTGAAGTATTTGGGAAAATT	CCATCTTTAACAAAAATCTTTAAATAACTTTTTCAAC
GRP78, R1	GAGAAGAAAAAGTTTAGATTTTATAG	AAACACCCCAATAAATCAATC

[a] Enhancer/region.

targeting histone H3 (ab1791; Abcam, Cambridge, MA), acetylated histone H3, Lys-9 and Lys-14 (06-599; Upstate Biotechnology Inc., Lake Placid, NY), dimethyl histone H3, Lys-4 (07-030; Upstate Biotechnology Inc.), the AR (N-20; Santa Cruz Biotechnology, Santa Cruz, CA), and GATA-2 (H-116; Santa Cruz Biotechnology). ChIP DNA was quantified by real-time qPCR using the Kapa SYBR Fast qPCR kit (Kapa, Woburn, MA) and the DNA Engine Opticon System (Bio-Rad, Hercules, CA). The qPCR assays were carried out using an arbitrary standard curve made from sonicated LNCaP cells genomic DNA to enable direct comparison across different primer sets. Data are represented as the average ± the standard error of the mean (SEM) from two independent experiments. All primers used for ChIP have a 60°C annealing temperature and are detailed in Table 1. *P* values of differences in the percentage of the input between primer sets 1 and 3 were calculated using SAS (analysis of variance [ANOVA]) considering the two experiments and PCR replicates as independent variables. *P* values of <0.05 are displayed in Fig. 2.

RNA isolation and qPCR analysis of androgen-responsive genes and *GATA-2*. Total RNA was extracted from DHT- or ethanol-treated control LNCaP or LAPC4 cells at the indicated time points using TRIzol (Invitrogen, Carlsbad, CA) and treated with DNase I (Invitrogen) according to the manufacturer's instructions. cDNA was prepared from 1 μg RNA using Superscript III reverse transcriptase (Invitrogen), and qPCR analysis for androgen-responsive genes

and *GATA-2* was conducted using SYBR green KAPA master mix and primers previously described (20, 22). Five microliters of sample was used for each qPCR. The relative amount of transcript was calculated by the cycle threshold method and normalized to the endogenous reference (glyceraldehyde 3-phosphate dehydrogenase [GAPDH]). The calibrator sample was randomly chosen from the ethanol-treated cells. The relative amount of target gene expression for each sample was calculated and plotted as the average ± the SEM from two or three independent experiments.

NOMe-Seq analysis of enhancers. Nucleosome occupancy and endogenous methylation at enhancer regions were determined as previously described (31), with minor modifications. Briefly, chromatin was isolated from 200,000 cells treated for 4 h or 16 h with DHT or ethanol (LNCaP and LAPC4) or left untreated (IMR90). Chromatin was incubated for 7.5 min with 200 U of enzyme GpC methylase (M.CviPI; New England BioLabs), which methylates GpC sites, followed by another 7.5 min of incubation with 100 U of M.CviPI. DNA was extracted and bisulfite converted using the EPITEC Bisulfite kit (Qiagen, Valencia, CA), and PCR fragments were cloned for sequencing of individual molecules.

PCR amplification of enhancer regions, cloning, and sequence analysis. The sequences of the primer sets used to investigate the enhancer regions are shown in Table 1. Enhancer regulatory regions were PCR amplified from bisulfite-converted DNA and cloned using the TOPO TA cloning kit (Invitrogen). Col-
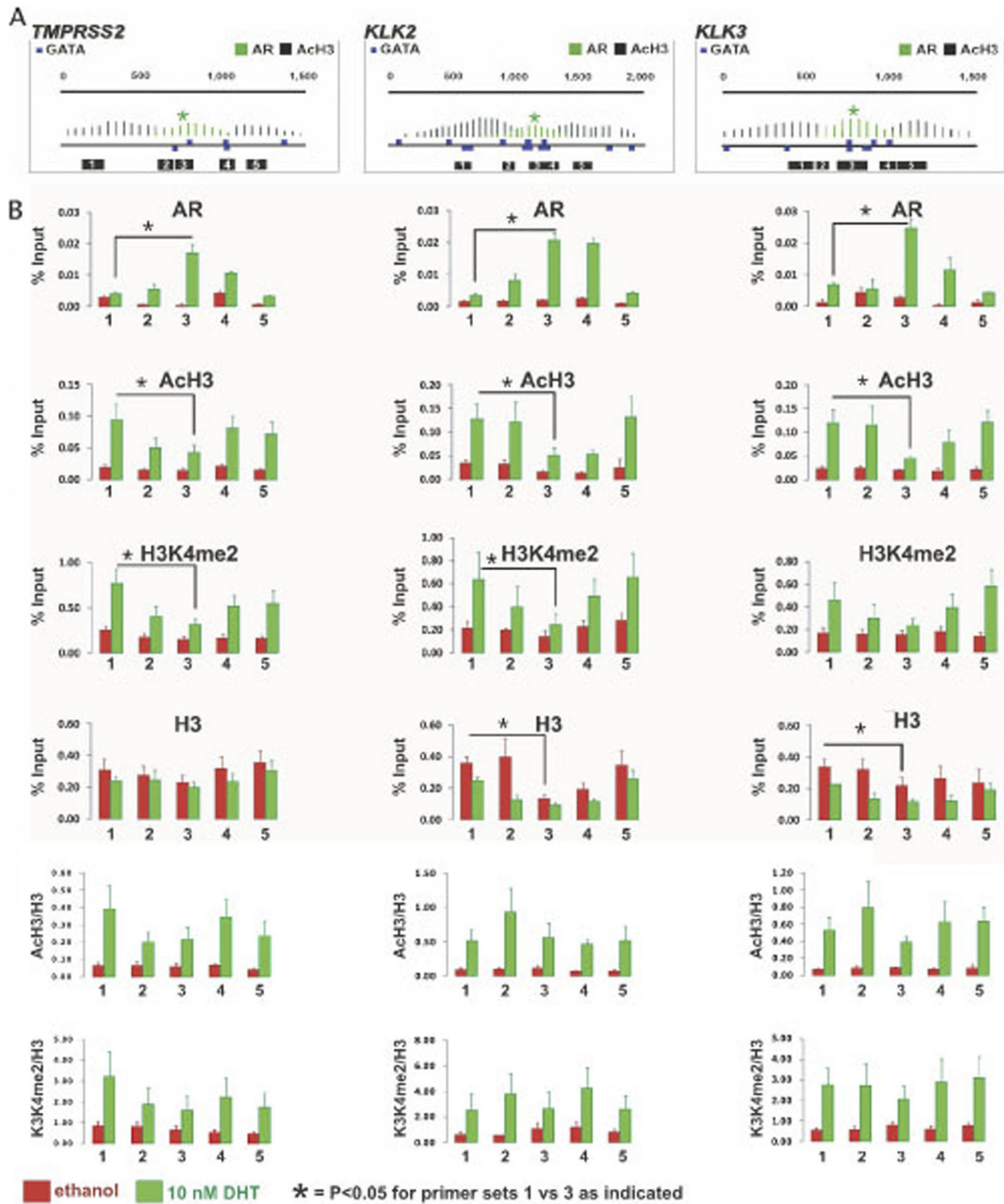
FIG. 2. Fine mapping of AR occupancy and histone modifications at the *TMPRSS2*, *KLK2*, and *KLK3* enhancers using ChIP-qPCR. (A) Five regions (black boxes 1 to 5) encompassing AR-occupied (green) and AcH3-modified (red) regions identified by ChIP-Seq were investigated by ChIP-qPCR analysis. Also shown are the locations of the functional AR elements (AREs, green star) and predicted GATA-2 binding sites (blue rectangles). (B) Site-specific ChIPs of AR, AcH3, H3K4me2, and H3 are presented as the average percentage of the input ± the SEM or as the average ratio to H3 ± the SEM of two independent experiments, in each case analyzed in duplicate or triplicate by qPCR. *P* values of percentages of the input between primer sets 1 and 3 were calculated using SAS (ANOVA) considering the two experiments and PCR replicates as independent variables. ∗, *P* < 0.05.

onies were screened for positive clones, and at least 15 positive clones per amplicon were sequenced per experiment. Results shown represent two independent biological replicates. Sequences were analyzed using the BiQ analyzer software (4). Accessible regions (green bubbles) and inaccessible regions (white

bubbles, pink bar) were plotted as bubble charts. Statistical analysis (chi square) of the ethanol and DHT treatments was performed for one GpC site every 100 bp. The percentage of inaccessible molecules was calculated for every GpC site in the amplicon [percentage of inaccessibility = (number of inaccessible mole-

cules/total number of molecules) × 100], and the results were averaged over a distance of 100 bp and plotted.

MNase digestion and qPCR analysis of enhancer regions. MNase digestion was carried out as described by Gal-Yam et al. (12) without chromatin fractionation. Cell lysates were incubated at 37°C for 15 min with increasing amounts of MNase I to determine the amount of enzyme required to enrich for mononucleosomes. An MNase I level of 5 IU was found to be suitable (see Fig. 4A) and was used in further experiments. LNCaP cells were maintained for 3 days in charcoal-stripped serum (CSS) and treated with ethanol or 10 nM DHT for 4 h, followed by MNase digestion. MNase-treated DNA was subjected to qPCR analysis using SYBR green KAPA master mix. Untreated, sonicated DNA was used as a control. Enhancer regions were investigated using 3 primer sets selected from our ChIP analysis. Primers were located within the nucleosome-depleted region (P3) and within the two flanking nucleosome-occupied regions (P2 and P5), as determined by NOMe-Seq. The qPCR assays were carried out using standard curves for each primer set made from sonicated LNCaP cells genomic DNA. Results are presented as quantities relative to the most abundant amplicon for each primer set (RQ). Results are shown as the averages of two independent experiments.

GATA-2 knockdown. LnCaP cells were transfected with predesigned SMART-pool small interfering RNA (siRNA) reagents against GATA-2 and nontargeted (control) siRNA (Dharmacon, Lafayette, CO) as previously described, with minor modifications. Briefly, 2 × 10^5 cells/well were plated in six-well plates and grown in phenol red-free RPMI 1640 containing 5% CSS for 2 days. Cells were transfected with the siRNA duplexes at a final concentration of 100 nM using Oligofectamine reagent (Invitrogen) according to the manufacturer's instructions. After transfection, cells were grown in phenol red-free RPMI 1640 containing 5% CSS for 48 h and then treated with the ethanol vehicle for additional 4 h. Cells were harvested and processed for NOMe-Seq analyses. Total RNA and protein extractions were also conducted to verify knockdown efficiency.

Western blot analysis. Immunoblotting was performed as previously described (19, 24) using an antibody against GATA-2 (H116) from Santa Cruz Biotechnology, Santa Cruz, CA. Anti-histone H3 antibody (Abcam, San Francisco, CA) was used as a loading control.

Data analysis. Statistical significance was determined by ANOVA, Student's t test or chi-square test as appropriate; P values of <0.05 were considered to be significant.

RESULTS

ChIP-Seq analysis of DHT-treated LNCaP cells shows that about 20% of all AR-occupied regions, including the *TMPRSS2*, *KLK2*, and *KLK3* enhancers, are flanked by AcH3 nucleosomes. Histone modifications surrounding transcription factor binding sites (18, 21) and local nucleosome positioning and displacement patterns provide information about the functional states of chromatin (13, 17). In prostate cancer cells, functionally significant chromatin signatures converge at AR-occupied regions, since it is known that the AR drives the disease (6). We aligned data obtained from a ChIP-Seq analysis of AR occupancy and histone AcH3 modification in LNCaP cells treated for 4 h with the natural AR ligand DHT. Figure 1A depicts 4,357 highly significant LNCaP cell AR-occupied regions (gray) and the fraction of AR-occupied regions overlapping a significant AcH3 peak at various distances (blue). About 20% of the AR-occupied regions were associated with AcH3; remarkably, a 200- to 400-bp area surrounding the apex of the AR peak displayed a very low number of AcH3 reads, possibly defining an NDR. In contrast, the flanking regions had the highest number of AcH3 reads and showed two well-defined peaks corresponding to two well-positioned acetylated nucleosomes. This pattern is highly reminiscent of that observed in other regulatory regions, such as promoters (36) and CTCF binding sites (11), and the fact that it is present in a large number of AR-occupied regions suggests that it may

play a role in the expression of target genes controlled by an important group of enhancers.

We selected to study in detail the enhancers of three well-established AR target genes, namely, *TMPRSS2*, *KLK2*, and *KLK3*/*PSA*. The *TMPRSS2* enhancer region is located approximately 13.5 kb upstream of the transcriptional start site and contains a noncanonical AR binding site. ChIP-Seq of AcH3 and AR occupancy in DHT-treated LNCaP cells showed two clear AcH3 peaks, flanking the AR binding site (arrow) at the *TMPRSS2* enhancer (Fig. 1B). Other androgen-occupied regions at this locus were not studied further. The *KLK3* enhancer is located between 5.8 and 3.7 kb upstream of the transcriptional start site, and the *KLK2* enhancer spans the region situated between 4.4 and 3.8 kb from the transcriptional start site (27). As previously reported (3), and similar to the *TMPRSS2* enhancer, two clear AcH3 peaks were found to flank the AR binding site at the *KLK2* and *KLK3* enhancers (Fig. 1B). These results suggest that, at the enhancers of androgen-responsive genes, AR is bound to an NDR which is flanked by two well-positioned nucleosomes containing AcH3. From these results, however, it is unclear whether the AcH3-free region may contain native unmodified histones or whether the proposed NDR precedes or follows AR binding.

AR recruitment leads to enrichment of AcH3 and H3K4me2 at the *TMPRSS2*, *KLK2*, and *KLK3* enhancers. To validate our ChIP-Seq observations, we analyzed gene expression, histone acetylation and methylation, and AR occupancy at the chosen three AR enhancer loci. As expected, 4 h of treatment with DHT significantly increased the *TMPRSS2*, *KLK2*, and *KLK3* mRNA levels in LNCaP cells compared to those in hormone-deprived cells (Fig. 1C, left panel). Further increases were observed after 16 h of treatment for all three genes (Fig. 1C, right panel).

Site-specific ChIP-qPCR analyses of AR occupancy, AcH3, H3K4me2 modifications, and native histone H3 were conducted at the *TMPRSS2*, *KLK2*, and *KLK3* enhancers. Five primer sets (Table 1) were used to map the AR-occupied regions and AcH3 peaks at the enhancers. Figure 2A displays a detailed image of the ChIP-Seq AcH3 (black ticks) and AR (green ticks) signals in LNCaP cells treated for 4 h with DHT and the relative positions of the five ChIP primer sets (P1 to P5) for each locus. ChIP analysis of AR occupancy (Fig. 2B) in DHT-treated LNCaP cells (green) shows a pattern similar to that observed in our ChIP-Seq data for all three enhancer regions. Significantly higher ($P < 0.05$) AR occupancy (green bars) was detected in the regions mapped by primer set P3 for at all three loci, than in the regions mapped by primer set P1 (located at the edge of enhancers). In contrast, negligible to no AR occupancy was observed in hormone-deprived cells (Fig. 2, red bars), indicating that AR binds to these loci only in the presence of DHT, a phenotype well known for androgen-dependent LNCaP cells. In agreement with the ChIP-Seq findings, AcH3 increased at the enhancers after DHT treatment (green bars) in a bimodal fashion, with two acetylation peaks in the regions mapped by primer sets P1, P4, and P5 for *TMPRSS2* and by primer sets P1, P2, and P5 for *KLK2* and *KLK3* (Fig. 2). AcH3 enrichment was significantly higher ($P < 0.05$) in the region mapped by primer set P1 (located at the AR binding site) than in the region mapped by primer set P3 for all three enhancers. Also in agreement with the ChIP-Seq analy-

sis, we found that the area corresponding to AR binding contained lower levels of AcH3. Hormone-deprived cells displayed very low acetylation across the five primer sets (red bars). Similarly, H3K4me2 was enriched in a bimodal pattern only in DHT-treated samples. H3K4me2 enrichment was significantly higher ($P < 0.05$) in the region mapped by primer set P1 than in the region mapped by primer set P3 for the *TMPRSS2* and *KLK2* enhancers. Finally, H3 was detected at higher levels in hormone-deprived samples at all three enhancers than in DHT-treated ones. The *KLK2* enhancer showed a clear bimodal pattern of distribution of H3 in the androgen-deprived samples. Significant differences were found between primer set P1 and primer set P3, suggesting the presence of an NDR in the hormone-deprived sample. Such a pattern was not readily apparent for the *TMPRSS2* and *KLK3* enhancers, although significant differences in H3 enrichment were found between primer set P1 and primer set P3 at the *KLK3* enhancer. When corrected for H3 levels (Fig. 2B, bottom panels), AcH3 levels were the same across all regions in the absence of DHT for all the enhancers; upon hormone treatment, AcH3 enrichment was observed in the regions flanking the AR binding site. In contrast, the levels of H3K4me2 corrected for H3 levels in the absence or presence of hormone at all enhancers were different than those shown when data were presented as percentages of the input, indicating that the observed depletion of H3K4me2 (when presented as a percentage of the input) simply reflected the presence of histones at the sites. The dramatic increase in AcH3 and H3K4me2 at all sites after DHT treatment more clearly demonstrated that the modifications occurred as a consequence of DHT treatment.

A percentage of *TMPRSS2*, *KLK2*, and *KLK3* enhancer modules displays NDRs in the absence of ligand. The results from the *KLK2* and *KLK3* enhancers were intriguing, particularly since it has recently been proposed that nucleosomes occupy AR enhancer regions in the absence of DHT (14). A possible explanation for the differences we observed between enhancers in terms of nucleosome positioning as determined by H3 ChIP analysis is the limited resolution level of the assay. To better resolve the pattern of nucleosome positioning and displacement in response to hormone treatment, we performed a high-resolution, single-molecule analysis named NOMe-Seq. This method is based on DNA accessibility to the 40,000-Da M.CviPI molecule, which methylates cytosines at GpC dinucleotides, and has been successfully used to establish nucleosome positions at promoters regions (23, 45). The advantage of NOMe-Seq analysis over traditional assays is that it allows the investigation of nucleosome position and endogenous methylation in the same molecule in CpG-poor regions (23) such as enhancers and without the biases previously reported for MNase I (2, 8). In addition, NOMe-Seq provides a digital readout of nucleosome positioning, thereby allowing direct comparison between treatments. Because NOMe-Seq relies on GC density, loss of resolution may be observed in extremely GC-poor regions. However, the three AR enhancers analyzed in this study have reasonably good GC densities, as do the majority of the gene-rich regions of the genome (28, 42), and therefore optimal resolution for the NOMe-Seq assay was expected. We designed two overlapping sets of primers (Table 1) lacking both GpC and CpG sites to eliminate amplification biases, which covered the full enhancer and additional neigh-

boring regions of *TMPRSS2*, *KLK2*, and *KLK3/PSA* (Fig. 3A). Primer location was based both on the coordinates of previously characterized enhancers (32, 37, 43, 47) and on the locations of AR-enriched peaks as determined in our genome-wide ChIP-Seq data (Fig. 1A). The results represent two independent experiments per time point and show a clear M.CviPI-accessible region (teal) in the hormone-deprived sample for all three enhancers (Fig. 3A). However, the degree of accessibility to M.CviPI differed among the regions, with the *KLK2* enhancer being the most accessible (41% of enhancer modules being nucleosome depleted), the *TMPRSS2* enhancer moderately accessible (26%), and the *KLK3* enhancer the least accessible (14%) (Fig. 3A and B). The observed accessible regions were large enough to accommodate at least one nucleosome, showing that even in the absence of androgens, some enhancer modules have NDRs. After 4 h of treatment with DHT (Fig. 3A and B), a significant increase in the number of accessible modules was observed at all three enhancers. Interestingly, the size (footprint) of the NDRs was not appreciably altered. The increase in numbers relative to the control sample was also differential and mirrored the pattern observed for the hormone-deprived samples as follows: *TMPRSS2*, 34%; *KLK2*, 27.2%; *KLK3*, 17.5% (Fig. 3B). In addition, M.CviPI accessibility in both hormone-deprived and DHT-treated samples was observed after 16 h in culture for all three enhancers (Fig. 3C).

To confirm nucleosome depletion at the AR binding site in the absence of hormone, we carried out MNase digestion followed by qPCR analysis of the *TMPRSS2* and *KLK2* enhancers in LNCaP cells as previously reported (12, 30). We selected three primer sets (P2, P3, and P5) from the five used for our ChIP analyses (Fig. 2), which covered the nucleosome-depleted (P3) enhancer region and two nucleosome-occupied (P2, P5) enhancer regions, as previously established by NOMe-Seq (Fig. 3). We first determined that the amount of MNase enzyme suitable to enrich for mononucleosomes was 5 IU (Fig. 4A). MNase digestion of LNCaP cells treated with DHT or ethanol for 4 h (after exposure to CSS for 3 days) clearly show a decrease in amplified product in the ethanol-treated samples at both enhancer regions (Fig. 4B). However, MNase digestion was less sensitive than NOMe-Seq in detecting changes in nucleosome depletion as a result of DHT treatment. The P3 primer set used in this analysis was located within the NDR detected by NOMe-Seq, which, according to its size, can accommodate only one nucleosome. Therefore, the decrease in amplified product is likely to reflect true nucleosome depletion, in agreement with the NOMe-Seq results.

In the absence of ligand, a percentage of *TMPRSS2* and *KLK2* enhancer modules always shows NDRs and this percentage increases after short-term treatment with DHT. To evaluate the kinetics of nucleosome positioning at AR enhancers, we performed NOMe-Seq analysis after short-term exposure to DHT (Fig. 5). A small increase in *TMPRSS2* and *KLK2* expression was observed as early as 0.5 h after DHT treatment (Fig. 5A). Results from the NOMe-Seq analysis of *TMPRSS2* and *KLK2* enhancers (Fig. 5B to E) clearly show 39 to 50% accessibility to M.CviPI (teal) in the ethanol-treated control samples, independently of the time of exposure to ethanol (0.5 h or 2 h). Treatment with DHT induced a significant increase in the number of accessible enhancer modules as early as 0.5 h

FIG. 3. Nucleosome positioning in *TMPRSS2*, *KLK2*, and *KLK3* enhancers as determined by NOMe-Seq analysis. (A) Single-molecule analysis of nucleosome occupancy for *TMPRSS2*, *KLK2*, and *KLK3* enhancers. Maps show GpC site density and the location of the enhancer (green bar) in the regions analyzed. DNA modules showing methylase-accessible regions (teal bubbles, upper panel) were present in the ethanol-treated control in all three enhancers. After DHT treatment, more DNA modules showed increased accessibility (teal bubbles, bottom panel). A chi-square test was carried out for seven GpC sites, chosen every 100 bp and indicated by arrows (a to g) on the enhancer map. Significant differences in nucleosome depletion between ethanol- and DHT-treated samples were found for the *TMPRSS2* enhancer (c, $P = 0.0012$), the KLK2 enhancer (d, $P = 0.03$; e, $P = 0.00009$; f, $P = 0.014$; g, $P = 0.009$), and the KLK3/PSA enhancer (d, $P = 0.004$). (B) Percentage of inaccessible GpC sites after 4 h of DHT treatment. The average percentage of inaccessible GpC sites every 100 bp is shown. The ethanol-treated control sample (red curve) showed a variable range of accessibility across the enhancer regions analyzed. Treatment with DHT (green curve) broadened the range; the percent increase in accessibility between ethanol- and DHT-treated samples is shown. The position of the enhancer (green bar under the graph) and the locations of the primer sets (P1 to P5) used in the ChIP-qPCR analysis are also shown. Note that the peak of accessibility overlaps the AR binding region mapped by ChIP-qPCR analysis. (C) Percentage of inaccessible GpC sites after 16 h of DHT treatment. A similar pattern of accessibility was observed after 16 h of treatment with DHT.
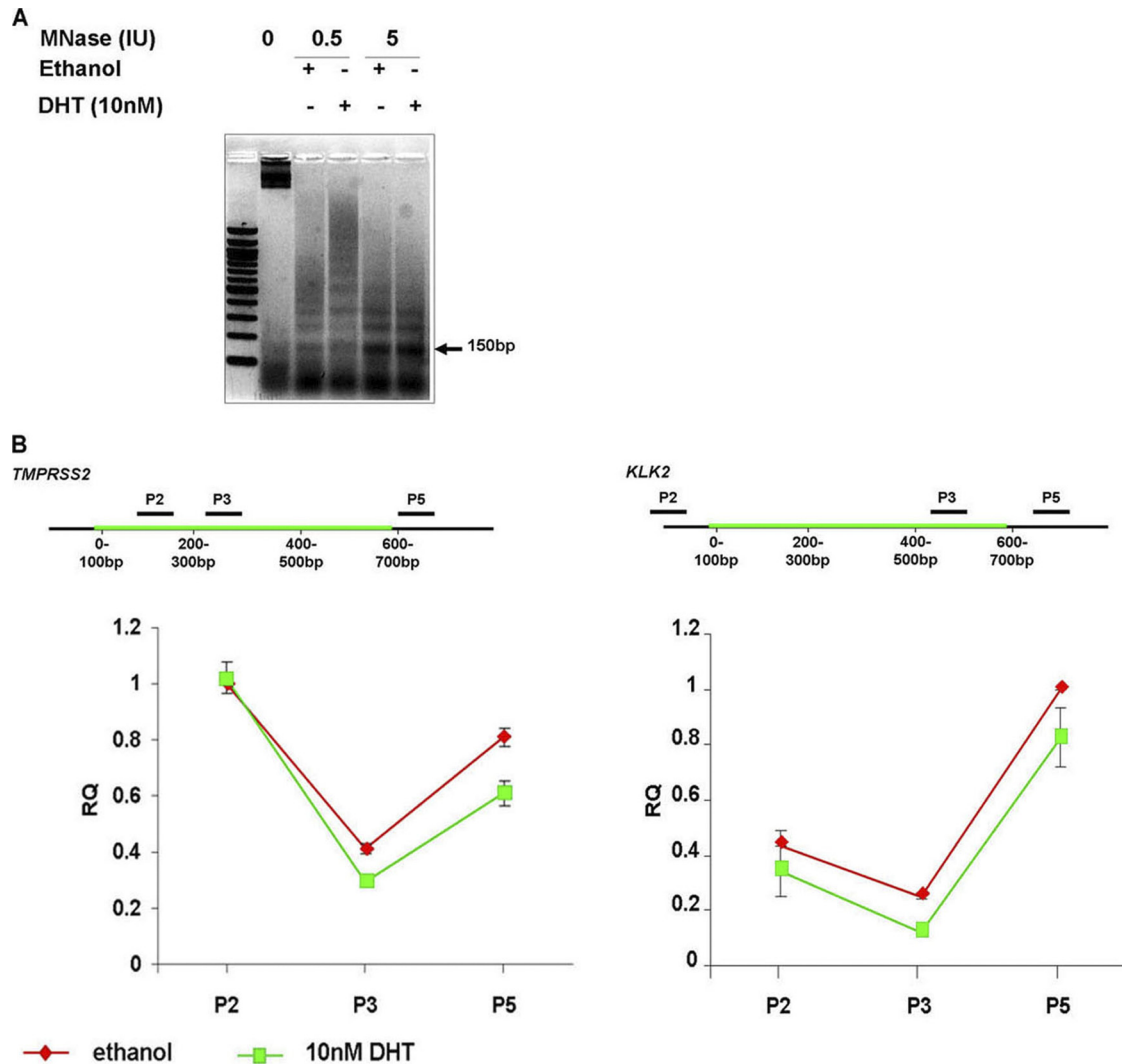
FIG. 4. MNase I analysis of the *TMPRSS2* and *KLK2* enhancers after 4 h of DHT treatment. (A) Representative depiction of MNase-digested samples. LNCaP cells were treated with ethanol or DHT for 4 h after the cultures had been exposed to CSS for 3 days; cells were lysed and chromatin was digested using 0.5 or 5 IU of MNase I for 15 min. Note that there is enrichment for mononucleosomes (arrow, 150 bp) after treatment with 5 IU MNase and this amount was selected for further studies. (B) MNase-treated DNA was subjected to qPCR analysis using 3 sets of primers selected from our ChIP analysis (P2, P3, and P5). Primers cover the nucleosome-depleted region (P3) and two nucleosome-occupied regions (P2 and P5) as determined by NOMe-Seq. The positions of the primer sets are indicated on the enhancer (green bar) maps. Note that nucleosome depletion (seen as a dip in the graphs) was observed in the ethanol-treated control sample, in agreement with the NOMe-Seq results. A small increase in nucleosome depletion was observed in the region mapped by P3 after DHT treatment. The average results from two independent experiments are shown.

posttreatment without affecting the size (footprint) of the NDRs, as was observed at later time points. The maximum increase in the number of accessible enhancer modules at the *TMPRSS2* enhancer (61%) was observed 0.5 h after exposure to DHT (Fig. 5B and C). At the *KLK2* enhancer, this value increased to 17.5% after 0.5 h of DHT exposure (Fig. 5B and 4C) and 21.7% after 2 h of exposure to DHT (Fig. 4D and E), which was similar to that observed after 4 h of treatment. These results suggest that nucleosome depletion in response to DHT treatment occurs shortly after DHT stimulation and coincides with AR occupancy.

NDRs are present after long-term androgen withdrawal. The NDR detected in the hormone-deprived sample could be caused by a transient short memory of the AR presence due to recent exposure (3 days) of LNCaP cells to androgens. To evaluate this possibility, we cultured cells in CSS for 7 days (i.e., longer time of hormone deprivation) prior to the 4-h treatment with DHT (Fig. 6). Our results indicate that even after prolonged hormone deprivation, the NDR is maintained at some of the *TMPRSS2* enhancer modules in the hormone-deprived sample (Fig. 6A and B), making it unlikely that the NDR is caused by a transient memory of the prior AR presence. In addition, prolonged hormone deprivation did not affect the response to DHT (Fig. 6A and B) and an 18% increase in accessibility relative to that in the hormone-deprived sample was observed.

Nucleosome positioning analyses of LAPC4 and IMR90 cells. To determine whether the patterns of nucleosome posi-
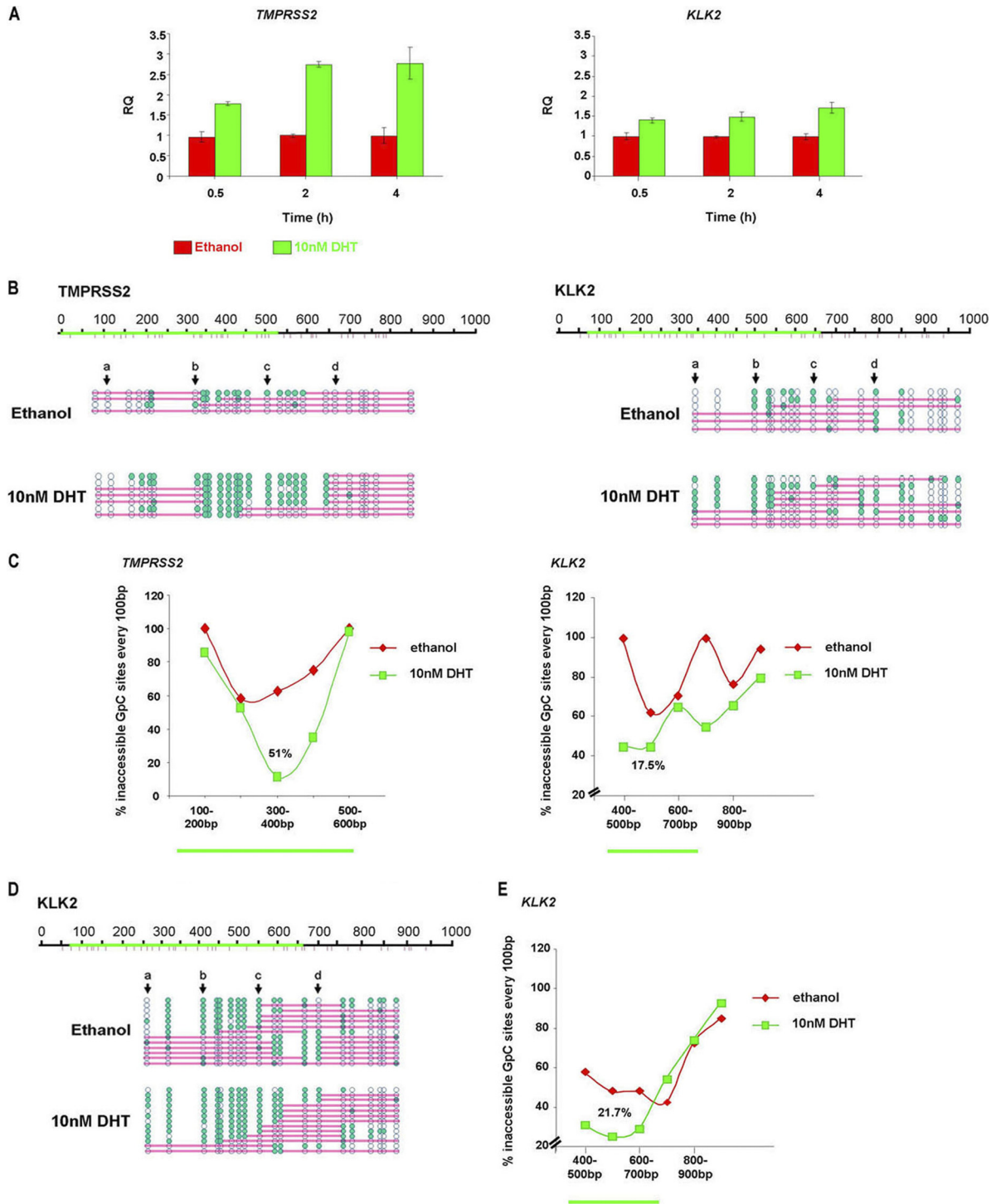
FIG. 5. NOMe-Seq analysis of nucleosome occupancy for *TMPRSS2* and *KLK2* enhancers after short-term DHT treatment. All cultures were exposed to CSS for 3 days prior to the start of the experiments. (A) qPCR analysis of *TMPRSS2* and *KLK2* mRNA levels after 0.5 h, 2 h, and 4 h of treatment with 10 nM DHT. Expression levels (RQ) are relative to GAPDH levels ($n = 2$). (B and D) Nucleosome positioning in LNCaP cells after 0.5 h (B) and 2 h (D) of treatment with DHT. Enhancer maps show GpC site density and the location of the enhancer (green bar) in the regions analyzed. DNA modules showing M.CviPI-accessible regions (teal bubbles) were present in the ethanol-treated control at both enhancers (upper panels). More modules became accessible to the methylase after DHT treatment (teal bubbles, bottom panels). Four GpC sites, chosen every 100 bp and indicated by arrows (a to d) on the enhancer map, were subjected to statistical analysis using the chi-square test. A significant difference in nucleosome depletion between ethanol- and DHT-treated samples was found for the *TMPRSS2* enhancer at position b ($P = 0.004$) and for the *KLK2* enhancer at position a ($P = 0.016$) after 0.5 h of treatment. No statistically significant difference was observed for the *KLK2* enhancer after 2 h of treatment with DHT. (C and E) Percentages of inaccessible GpC sites in LNCaP cells after 0.5 h (C) and 2 h (D) of treatment with DHT. The average percentage of inaccessible GpC sites every 100 bp is shown. Note that the ethanol-treated control sample (red curve) showed a variable range of accessibility across the enhancer regions analyzed. Treatment with DHT (green curve) broadened the range; the percent increase in accessibility between ethanol- and DHT-treated samples is shown.
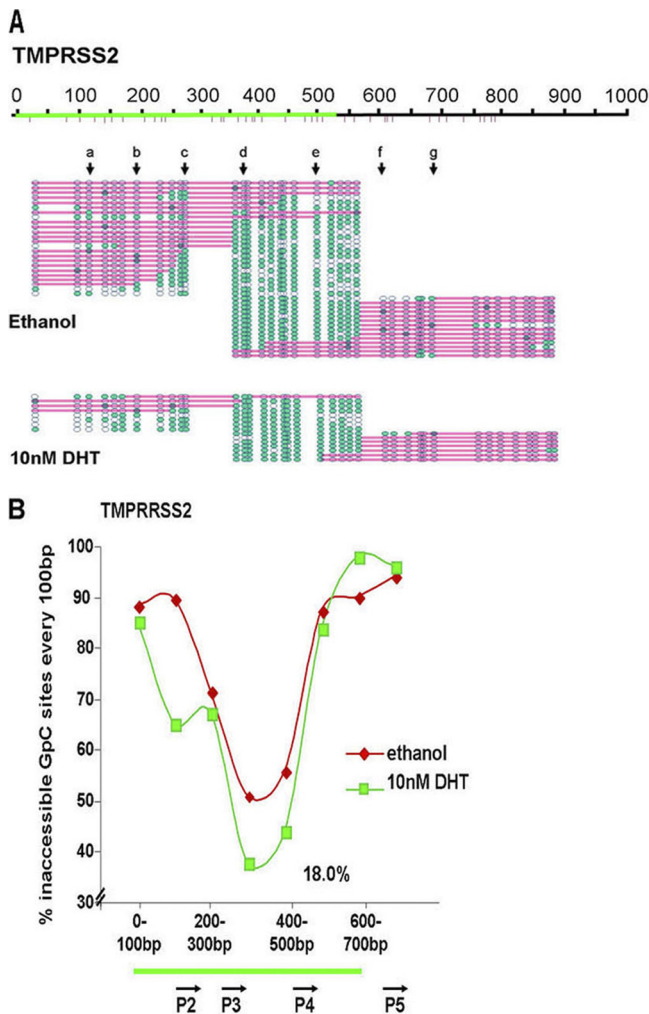
FIG. 6. Nucleosome positioning in the *TMPRSS2* enhancer as determined by NOMe-Seq analysis after extended androgen deprivation. LNCaP cells were cultured in CSS for 7 days and then treated with ethanol (control) or DHT (10 nM) for 4 h. (A) Single-molecule analysis of nucleosome occupancy for the *TMPRSS2* enhancers. Enhancer maps show GpC site density and the location of the enhancer (green bar) in the region analyzed. DNA modules showing M.CviPI-accessible regions (teal bubbles, upper panel) were present in the ethanol-treated control, and after DHT treatment, more DNA modules showed increased accessibility (teal bubbles, bottom panel). Seven GpC sites, chosen every 100 bp and indicated by arrows (a to g) in the enhancer map, were subjected to statistical analysis using the chi-square test. A significant difference in nucleosome depletion between ethanol- and DHT-treated samples was found for the *TMPRSS2* enhancer at position d ($P = 0.047$). (B) Percentage of inaccessible GpC sites after 4 h of DHT treatment. The average percentage of inaccessible GpC sites every 100 bp is shown. Note that the ethanol-treated control sample (red curve) also showed accessibility after extended androgen deprivation. Treatment with 10 nM DHT (green curve) broadened the range; the percent increase in accessibility between ethanol- and DHT-treated samples is apparent. The position of the enhancer relative to the accessibility region is shown as a green bar under the graph. The locations of the primer sets (P1 to P5, Fig. 2) used in the ChIP-qPCR analysis are also shown. Note that the peak of accessibility overlaps the AR binding region mapped by ChIP-qPCR analysis.

tioning were conserved among androgen-sensitive cell lines, we performed a NOMe-Seq analysis with LAPC4 cells, which express the wild-type AR (Fig. 7). Cells were treated with DHT or ethanol for 4 h after exposure to CSS for 2 days. The pattern of nucleosome occupancy for the *KLK2* enhancer (Fig. 7A and B) was comparable to that of LNCaP cells (Fig. 3A). Importantly, 75% of *KLK2* enhancer modules had NDRs in the ethanol-treated control samples. In contrast, the *TMPRSS2* enhancer was occupied by nucleosomes (pink bars) in the ethanol-treated sample (Fig. 7A and B), suggesting that accessibility of the enhancers in the absence of ligand may vary among androgen-responsive cell lines. DHT treatment increased the number of enhancer modules displaying NDRs without affecting the footprint size, as was also shown for LNCaP cells. The increase in enhancer accessibility in response to DHT was accompanied by increases in gene expression (Fig. 7C). The same enhancer regions in the human fibroblast cell line IMR90, which expresses neither *TMPRSS2* nor *KLK2* (Oncomine; Compendia Bioscience, Ann Arbor, MI), showed complete nucleosome occupancy (Fig. 7D). On the other hand, the *GRP78*/*HSPA5* promoter, which is expressed in these cells (Oncomine; Compendia Bioscience, Ann Arbor, MI), showed a pattern of M.CviPI accessibility typical of active promoters (Fig. 7D), as was previously reported by our group (12). The three enhancer regions were CpG poor and, as expected, showed very low endogenous methylation levels within the enhancer in both LNCaP and LAPC4 cells (data not shown).

The *TMPRSS2*, *KLK2*, and *KLK3* enhancers show GATA-2 enrichment in the absence of ligand. The AR, acting in concert with other (pioneer) transcription factors such as GATA-2, OCT-1, and FOXA1, mediates the expression of androgen-responsive genes. In particular, OCT1 and GATA-2 have been shown to regulate *TMPRSS2* and *KLK3* expression (33, 43), and GATA-2 has also been shown to regulate *KLK2* expression (5). FOXA1 and GATA-2 act as pioneer factors in the recruitment of AR, although FOXA1 appears to be recruited to a restricted number of sites (43). In yeast, the transcription factor RSC3 was shown to be required for the maintenance of an NDR in the proximal promoter region of a number of genes that contain the RSC3 binding motif (1). However, a similar role for transcription factors at promoters or in other regulatory regions has not been described in mammals.

Since pioneer factors are present at AR enhancers in the absence of DHT, we hypothesized that their binding affects the turnover rates of nucleosomes in these regions toward the nucleosome-depleted state, as previously suggested (29). To test this hypothesis, we used ChIP-qPCR to verify GATA-2 binding to the *TMPRSS2*, *KLK2*, and *KLK3* enhancers by ChIP. The results show that GATA-2 is enriched in all three enhancers irrespective of the presence of DHT (Fig. 8A), which is consistent with the presence of GATA response elements at all three loci (blue rectangles, Fig. 2A). Furthermore, we found that GATA-2 was particularly enriched at the NDRs. For instance, comparing the results of the GATA-2 ChIP analysis and nucleosome positioning at the *KLK2* enhancer makes it clear that the regions amplified by P3 and P4 show both the highest signal for GATA-2 binding (Fig. 8A, middle panel) and an NDR (Fig. 3B).

GATA-2 is important for NDR maintenance at the TPMRSS2 enhancer in the absence of hormone. Next, using
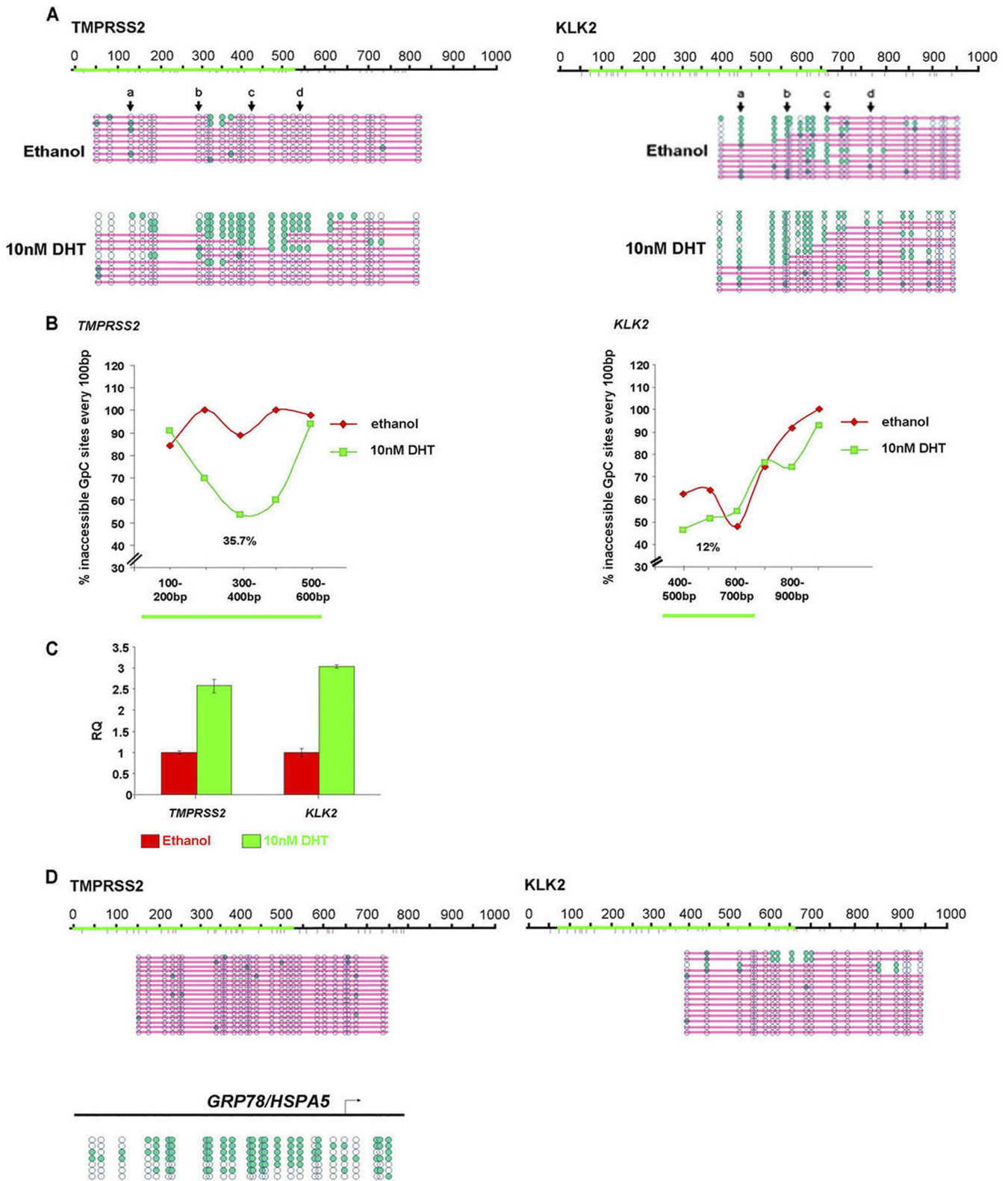
FIG. 7. NOMe-Seq analysis of nucleosome occupancy for *TMPRSS2* and *KLK2* enhancers in LAPC4 and IMR90 cells. Enhancer maps show GpC site density and the locations of the enhancers (green bar) in the regions analyzed. (A) LAPC4 cells were maintained in CSS for 2 days and treated with ethanol (control) or DHT for 4 h. DNA modules showing that M.CviPI-accessible regions (teal bubbles, upper panel) were present in the ethanol-treated control at the *KLK2* and *TMPRSS2* enhancers in LAPC4 cells (upper panel). Similar to LNCaP cells, increased DNA accessibility to the methylase was observed in both enhancers after 4 h of treatment with DHT (teal bubbles, bottom panel). Four (*TMPRSS2*) or five (*KLK2*) GpC sites, chosen every 100 bp and indicated by arrows (a to d, a to e) on the enhancer map, were subjected to statistical analysis

siRNA to knock down the levels of endogenous GATA-2 in LnCaP cells, we investigated the role of this pioneering factor in maintaining the NDRs at AR enhancers in the absence of hormone. A 70% decrease in *GATA-2* mRNA levels (Fig. 8, top panel) and a further decrease in protein levels (Fig. 8B, bottom panel) were observed in LnCaP cells after *GATA-2* knockdown. Analysis of nucleosome positioning by NOMe-Seq revealed that knockdown of *GATA-2* significantly ($P < 0.05$) decreased the accessibility of the *TMPRSS2* enhancer to M.CviPI by 44% but did not alter the accessibility of the *KLK2* and *KLK3* enhancers (Fig. 8C and D). However, after GATA-2 knockdown, a new accessible area was observed downstream of the *KLK3* enhancer. This area is smaller than a nucleosome and may reflect transcription factor loss (either GATA-2 or others). The results suggest a "pioneering" role for GATA-2 at some, but not all, AR enhancers and provide support for the hypothesis that pioneer factors help maintain enhancer accessibility for subsequent transcription factor binding and action.

DISCUSSION

Nucleosome positioning at promoter regions is being increasingly recognized as an important factor in the regulation of gene expression (34), and nucleosome turnover kinetics, "sliding," and "hopping" have been proposed to facilitate such regulation (29, 35). Nucleosomes affect the way transcription factors bind to their recognition sequences, thereby modulating transcription (2). Whereas some transcription factors may require NDRs for binding, others may bind with low affinity even if a nucleosome is present or bind with high affinity irrespective the presence or absence of a nucleosome. Binding of transcription factors to an NDR may confer the advantage of a quick response and allow low transcription factor titers to remain functional (2).

Here, using a combination of ChIP and a high-resolution, single-molecule nucleosome positioning assay, we show that, in LnCaP cells and in the absence of the AR ligand/hormone (DHT), the enhancers of androgen-responsive genes have NDRs whose locations overlap those of GATA-2-enriched regions. A similar pattern of nucleosome occupancy was found in another prostate cancer cell line, LAPC4, but not in human fibroblasts, suggesting that this might be a conserved feature of AR enhancers in androgen-sensitive cells. Treatment with DHT induces AR recruitment and increases the number of DNA enhancer modules displaying NDRs but not the size of the nucleosome-depleted area. Based on our results, we propose a model by which AR enhancers exist in an equilibrium in which the turnover rates of nucleosomes create a population of

enhancer modules with a clear NDR at any given time. DHT treatment, which recruits the AR to the sites, changes the equilibrium toward the nucleosome-depleted state, and as a consequence, more enhancer modules display NDRs. The increase in the number of modules showing NDRs was observed even at 0.5 h after DHT exposure, suggesting that the shift of the equilibrium toward a more nucleosome-depleted state is very rapid. The exact mechanism by which the NDRs are established and maintained in the absence of DHT is unknown. One possibility is that the NDRs are passively formed as a consequence of spontaneous DNA accessibility and maintained by the binding of transcription factors (29). Our data showing GATA-2 binding in the absence of DHT, as well as the disappearance of the NDR after *GATA-2* knockdown, at some but not all AR enhancers support this hypothesis. We propose that other factors may be required to displace the equilibrium toward a more nucleosome-depleted configuration after DHT treatment, a hypothesis that is in line with the model of factor cooperativity reviewed by Segal and Widom (38).

A recent study by He et al. (14) described a nucleosome-occupied region in the area corresponding to the AR binding site at the enhancers of androgen-responsive genes under hormone-deprived conditions, based on prediction algorithms built on MNase I digestion and ChIP-Seq data. Those authors also indicated that nucleosomes in that region contain the histone variant H2A.Z, which they suggested may destabilize those nucleosomes. However, the stability of the nucleosome was not tested. Although we did not analyze H2A.Z enrichment at the three well-characterized AR enhancers studied here, our analysis of nucleosome occupancy using NOMe-Seq clearly shows that NDRs do, in fact, exist in the absence of hormone. MNase analysis of LNCaP cells treated with ethanol or DHT for 4 h confirmed an NDR in ethanol-treated samples, in agreement with our NOMe-Seq results. Since we found that a given percentage of enhancer modules was inaccessible in both the presence and the absence of DHT, our data are consistent with the hypothesis that nucleosomes positioned at the center of the AR binding site may be more labile, perhaps as a consequence of carrying the H2A.Z histone variant, as proposed by He et al. (14). Our finding that more modules displayed NDRs after DHT treatment is entirely consistent with that of He et al. (14).

Our H3K4me2 ChIP data analysis is also in agreement with that reported by He et al. (14), who showed that two well-positioned nucleosomes containing this histone modification flank the AR binding site after DHT stimulation. However, both our native H3 and H3K4me2 ChIPs suggest that there is

---

using the chi-square test. A significant difference in nucleosome depletion between ethanol- and DHT-treated samples was found in the *TMPRSS2* enhancer at positions b ($P = 0.03$) and c ($P = 0.0115$); no significant differences between treatments were found for the *KLK2* enhancer. (B) Percentage of inaccessible GpC sites after 4 h of DHT treatment. The average percentage of inaccessible GpC sites every 100 bp is shown. Note that the ethanol-treated control sample (red curve) also showed accessibility after extended androgen deprivation. Treatment with 10 nM DHT (green curve) broadened the range; the percent increase in accessibility between ethanol- and DHT-treated samples is shown. The position of the enhancer relative to the accessibility region is shown as a green bar under the graph. (C) qPCR analysis of *TMPRSS2* and *KLK2* mRNA levels after 4 h of treatment of LAPC4 cells with 10 nM DHT. Expression is shown relative to GAPDH levels (RQ, $n = 2$). (D) IMR90 cells, which do not express *TMPRSS2* or *KLK2*, showed total inaccessibility to M.CviPI for both of the enhancers. In contrast, and as expected, the promoter region of the expressed gene *HSPA5/GRP78* (70-kDa heat shock protein 5/78-kDa glucose-regulated protein) was readily accessible to M.CviPI (teal bubbles).
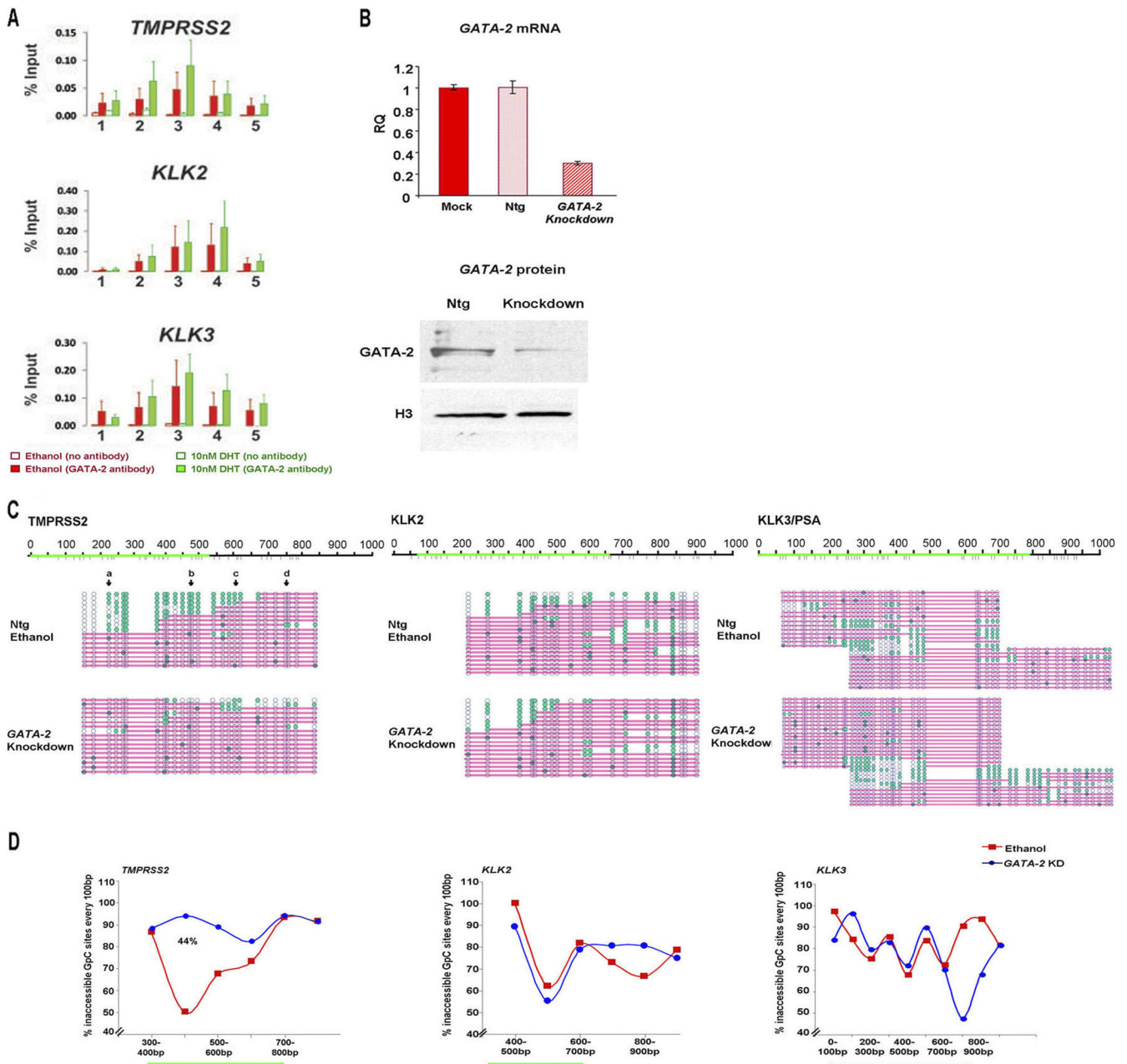
FIG. 8. GATA-2 occupancy at the *TMPRSS2*, *KLK2*, and *KLK3* enhancers and nucleosome positioning in LNCaP cells after GATA-2 knockdown. (A) GATA-2 occupancy was detected at all three enhancers in both ethanol-treated control cells (red solid bars) and DHT-treated cells (green solid bars), as shown by enrichment of immunoprecipitated DNA compared with the respective no-antibody controls (red and green open bars). Site-specific ChIPs (see Fig. 2) of GATA-2 are presented as the average percentage of the input ± the SEM of two independent experiments, in each case analyzed in duplicate or triplicate by qPCR. LNCaP cells were transfected with siRNA against GATA-2 or nontargeted siRNA (control); cells were maintained in CSS for 2 days and treated with ethanol for 4 h. (B) qPCR (upper panel) and Western blot (lower panel) analyses of *GATA-2* mRNA and protein levels after *GATA-2* knockdown. Mock-transfected cells and cells transfected with nontargeted (Ntg) siRNA were used as controls. Expression is shown relative to GAPDH levels (RQ, $n = 2$). A representative blot is shown. Histone H3 was used as a loading control. (C) Enhancer maps showing GpC site densities and the locations of the enhancers (green bar) in the regions analyzed. DNA modules showing M.CviPI-accessible regions (teal bubbles) were present in the nontargeted control at all enhancers. Note that accessibility after *GATA-2* knockdown was reduced only at the *TMPRSS2* enhancer. A chi-square test was carried out for the *TMPRSS2* enhancer at four GpC sites, chosen every 100 bp and indicated by arrows (a to d) on the enhancer map. Significant differences in nucleosome depletion between nontargeted control and *GATA-2* siRNA-treated samples were found for the *TMPRSS2* enhancer (a and b, $P < 0.05$). (D) Percentage of inaccessible GpC sites after *GATA-2* knockdown. The average percentage of inaccessible GpC sites every 100 bp is shown. Note that a 44% decrease in M.CviPI accessibility was observed for the *TMPRSS2* enhancer.

no enrichment of these marks at the central AR binding regions relative to the flanking sites in cells maintained in the absence of DHT, in agreement with the NOMe-Seq data reported in this report. The presence of NDRs at other AR enhancers in the absence of hormone remains to be elucidated; however, our results provide support for the hypothesis that a percentage of AR enhancer modules at a particular locus is primed to accept the transcription factor, even under hormone ablation conditions like those that exist in the course of treatment of advanced prostate cancer cases.

AR signaling is critical in all phases of prostate cancer, including disease initiation, androgen-dependent tumor growth, and the evolution of resistance to androgen ablation therapies (26). The mechanisms proposed to contribute to ablation-resistant growth of prostate cancer all involve reactivation of the AR under ablation conditions (reviewed in reference 46). A major mechanistic advance has been the realization that the ablation-resistant phenotype in many tumors is accompanied by the fusion of *TMPRSS2* (along with its AR enhancer) and *ETS* transcription factor genes, allowing AR stimulation of the powerful secondary transcription factor family (46) or by the expression of AR constitutively active splicing variants (40). Furthermore, the involvement of the AR in the ablation-resistant phenotype was clearly demonstrated by the disruption of AR expression, which inhibited the proliferation of ablation-resistant prostate cancer cells in the absence of androgens (48). AR expression was also shown to be necessary and sufficient to convert androgen-sensitive prostate cancer to an ablation-resistant state (7). These lines of evidence prove that aberrant AR signaling and its target genes are sufficient to cause prostate cancer and that under certain conditions the AR gene may be considered an oncogene.

The role of AR enhancers in prostate cancer represents the other side of the same coin. Enhancers activate gene expression independently of their orientation and are commonly scattered across large noncoding intervals, as well as within introns. It is also important to note that enhancers are often cell type specific (15), and in the case of prostate cancer, AR enhancers drive all phases of the disease, as discussed above. Work described in this report adds to the growing body of evidence demonstrating the pivotal role of the AR and its enhancers in the development of the ablation-resistant phenotype in prostate cancer. Our data showing that AR enhancers seem to be "primed" for or "receptive" to AR activity during hormone-depleted conditions underscore a possible mechanism by which they may become efficiently engaged by AR during the course of hormone ablation treatment of prostate cancer patients. Furthermore, our study points to AR enhancers as critical genomic regions with therapeutic potential to treat ablation-resistant prostate cancer.

ACKNOWLEDGMENTS

REFERENCES

1. **Badis, G., et al.** 2008. A library of yeast transcription factor motifs reveals a widespread function for Rsc3 in targeting nucleosome exclusion at promoters. Mol. Cell **32:**878–887.
2. **Bai, L., and A. V. Morozov.** 2010. Gene regulation by nucleosome positioning. Trends Genet. **26:**476–483.
3. **Berman, B. P., B. Frenkel, G. A. Coetzee, and L. Jia.** 2010. Androgen receptor responsive enhancers are flanked by consistently-positioned H3-acetylated nucleosomes. Cell Cycle **9:**2249–2250.
4. **Bock, C., et al.** 2005. BiQ Analyzer: visualization and quality control for DNA methylation data from bisulfite sequencing. Bioinformatics **21:**4067–4068.
5. **Böhm, M., W. J. Locke, R. L. Sutherland, J. G. Kench, and S. M. Henshall.** 2009. A role for GATA-2 in transition to an aggressive phenotype in prostate cancer through modulation of key androgen-regulated genes. Oncogene **28:**3847–3856.
6. **Carver, B. S., et al.** 2011. Reciprocal feedback regulation of PI3K and androgen receptor signaling in PTEN-deficient prostate cancer. Cancer Cell **19:**575–586.
7. **Chen, C. D., et al.** 2004. Molecular determinants of resistance to antiandrogen therapy. Nat. Med. **10:**33–39.
8. **Chung, H. R., et al.** 2010. The effect of micrococcal nuclease digestion on nucleosome positioning data. PLoS One **5:**e15754.
9. **Deal, R. B., and S. Henikoff.** 2010. Capturing the dynamic epigenome. Genome Biol. **11:**218.
10. **Donkena, K. V., H. Yuan, and C. Y. Young.** 2010. Recent advances in understanding hormonal therapy resistant prostate cancer. Curr. Cancer Drug Targets **10:**402–410.
11. **Fu, Y., M. Sinha, C. L. Peterson, and Z. Weng.** 2008. The insulator binding protein CTCF positions 20 nucleosomes around its binding sites across the human genome. PLoS Genet. **4:**e1000138.
12. **Gal-Yam, E. N., et al.** 2006. Constitutive nucleosome depletion and ordered factor assembly at the GRP78 promoter revealed by single molecule footprinting. PLoS Genet. **2:**e160.
13. **Goh, W. S., Y. Orlov, J. Li, and N. D. Clarke.** 2010. Blurring of high-resolution data shows that the effect of intrinsic nucleosome occupancy on transcription factor binding is mostly regional, not local. PLoS Comput. Biol. **6:**e1000649.
14. **He, H. H., et al.** 2010. Nucleosome dynamics define transcriptional enhancers. Nat. Genet. **42:**343–347.
15. **Heintzman, N. D., and B. Ren.** 2009. Finding distal regulatory elements in the human genome. Curr. Opin. Genet. Dev. **19:**541–549.
16. **Heintzman, N. D., et al.** 2007. Distinct and predictive chromatin signatures of transcriptional promoters and enhancers in the human genome. Nat. Genet. **39:**311–318.
17. **Henikoff, S.** 2008. Nucleosome destabilization in the epigenetic regulation of gene expression. Nat. Rev. Genet. **9:**15–26.
18. **Jia, L., et al.** 2008. Genomic androgen receptor-occupied regions with different functions, defined by histone acetylation, coregulators and transcriptional capacity. PLoS One **3:**e3645.
19. **Jia, L., et al.** 2004. Androgen receptor signaling: mechanism of interleukin-6 inhibition. Cancer Res. **64:**2619–2626.
20. **Jia, L., et al.** 2003. Androgen receptor activity at the prostate specific antigen locus: steroidal and non-steroidal mechanisms. Mol. Cancer Res. **1:**385–392.
21. **Jia, L., et al.** 2009. Functional enhancers at the gene-poor 8q24 cancer-linked locus. PLoS Genet. **5:**e1000597.
22. **Jia, L., et al.** 2006. Locus-wide chromatin remodeling and enhanced androgen receptor-mediated transcription in recurrent prostate tumor cells. Mol. Cell. Biol. **26:**7331–7341.
23. **Kelly, T. K., et al.** 2010. H2A.Z maintenance during mitosis reveals nucleosome shifting on mitotically silenced genes. Mol. Cell **39:**901–911.
24. **Kim, J., L. Jia, W. D. Tilley, and G. A. Coetzee.** 2003. Dynamic methylation of histone H3 at lysine 4 in transcriptional regulation by the androgen receptor. Nucleic Acids Res. **31:**6741–6747.
25. **Kim, T. K., et al.** 2010. Widespread transcription at neuronal activity-regulated enhancers. Nature **465:**182–187.
26. **Lamont, K. R., and D. J. Tindall.** 2010. Androgen regulation of gene expression. Adv. Cancer Res. **107:**137–162.
27. **Lawrence, M. G., J. Lai, and J. A. Clements.** 2010. Kallikreins on steroids: structure, function, and hormonal regulation of prostate-specific antigen and the extended kallikrein locus. Endocr. Rev. **31:**407–446.
28. **Lercher, M. J., A. O. Urrutia, A. Pavlicek, and L. D. Hurst.** 2003. A unifi-

cation of mosaic structures in the human genome. Hum. Mol. Genet. **12:** 2411–2415.

29. **Li, G., M. Levitus, C. Bustamante, and J. Widom.** 2005. Rapid spontaneous accessibility of nucleosomal DNA. Nat. Struct. Mol. Biol. **12:**46–53.

30. **Lin, J. C., et al.** 2007. Role of nucleosomal occupancy in the epigenetic silencing of the MLH1 CpG island. Cancer Cell **12:**432–444.

31. **Miranda, T. B., T. K. Kelly, K. Bouazoune, and P. A. Jones.** 1 January 2010, posting date. Methylation-sensitive single-molecule analysis of chromatin structure. Curr. Protoc. Mol. Biol. **21.17:**1–16. doi:10.1002/0471142727.mb2117s89.

32. **Mitchell, S. H., P. E. Murtha, S. Zhang, W. Zhu, and C. Y. Young.** 2000. An androgen response element mediates LNCaP cell dependent androgen induction of the hK2 gene. Mol. Cell. Endocrinol. **168:**89–99.

33. **Perez-Stable, C. M., A. Pozas, and B. A. Roos.** 2000. A role for GATA transcription factors in the androgen regulation of the prostate-specific antigen gene enhancer. Mol. Cell. Endocrinol. **167:**43–53.

34. **Radman-Livaja, M., and O. J. Rando.** 2010. Nucleosome positioning: how is it established, and why does it matter? Dev. Biol. **339:**258–266.

35. **Ranjith, P., J. Yan, and J. F. Marko.** 2007. Nucleosome hopping and sliding kinetics determined from dynamics of single chromatin fibers in Xenopus egg extracts. Proc. Natl. Acad. Sci. U. S. A. **104:**13649–13654.

36. **Schones, D. E., et al.** 2008. Dynamic regulation of nucleosome positioning in the human genome. Cell **132:**887–898.

37. **Schuur, E. R., et al.** 1996. Prostate-specific antigen expression is regulated by an upstream enhancer. J. Biol. Chem. **271:**7043–7051.

38. **Segal, E., and J. Widom.** 2009. What controls nucleosome positions? Trends Genet. **25:**335–343.

39. **Sharma, S., T. K. Kelly, and P. A. Jones.** 2010. Epigenetics in cancer. Carcinogenesis. **31:**27–36.

40. **Sun, S., et al.** 2010. Castration resistance in human prostate cancer is conferred by a frequently occurring androgen receptor splice variant. J. Clin. Invest. **120:**2715–2730.

41. **van Berkum, N. L., and J. Dekker.** 2009. Determining spatial chromatin organization of large genomic regions using 5C technology. Methods Mol. Biol. **567:**189–213.

42. **Versteeg, R., et al.** 2003. The human transcriptome map reveals extremes in gene density, intron length, GC content, and repeat pattern for domains of highly and weakly expressed genes. Genome Res. **13:**1998–2004.

43. **Wang, Q., et al.** 2007. A hierarchical network of transcription factors governs androgen receptor-dependent prostate cancer growth. Mol. Cell **27:**380–392.

44. **Wang, Z., et al.** 2008. Combinatorial patterns of histone acetylations and methylations in the human genome. Nat. Genet. **40:**897–903.

45. **Wolff, E. M., et al.** 2010. Hypomethylation of a LINE-1 promoter activates an alternate transcript of the MET oncogene in bladders with cancer. PLoS Genet. **6:**e1000917.

46. **Yamaoka, M., T. Hara, and M. Kusaka.** 2010. Overcoming persistent dependency on androgen signaling after progression to castration-resistant prostate cancer. Clin. Cancer Res. **16:**4319–4324.

47. **Yu, D. C., G. T. Sakamoto, and D. R. Henderson.** 1999. Identification of the transcriptional regulatory sequences of human kallikrein 2 and their use in the construction of calydon virus 764, an attenuated replication competent adenovirus for prostate cancer therapy. Cancer Res. **59:**1498–1504.

48. **Zegarra-Moro, O. L., L. J. Schmidt, H. Huang, and D. J. Tindall.** 2002. Disruption of androgen receptor function inhibits proliferation of androgen-refractory prostate cancer cells. Cancer Res. **62:**1008–1013.